DOI: 10.1002/chem.200800039

# The Bound Conformation of Microtubule-Stabilizing Agents: NMR Insights into the Bioactive 3D Structure of Discodermolide and Dictyostatin**

**Angeles Canales,[a] Ruth Matesanz,[a] Nicola M. Gardner,[b] José Manuel Andreu,[a] Ian Paterson,[b] J. Fernando Díaz,*[a] and Jesús Jiménez-Barbero*[a]**

**Abstract:** A protocol based on a combination of NMR experimental data with molecular mechanics calculations and docking procedures has been employed to determine the microtubule-bound conformation of two microtubule-stabilizing agents, discodermolide (DDM) and dictyostatin (DCT). The data indicate that tubulin in assembled microtubules recognizes DDM through a conformational selection process, with minor changes in the molecular skeleton between the major conformer in water solution and that bound to assembled microtubules. For DCT, the deduced bound geometry presents some key conformation differences around certain torsion angles, with respect to the major conformer in solution, and still displays mobility even when bound. The bound conformer of DCT resembles that of DDM and provides very similar contacts with the receptor. Competition experiments indicate that both molecules compete with the taxane-binding site. A model of the binding mode of DDM and DCT to tubulin is proposed.

**Keywords:** anticancer agents · conformation analysis · microtubules · molecular modeling · molecular recognition

## Introduction

A major challenge of contemporary medicine is in cancer chemotherapy. A cancerous cell is exquisitely well adapted for survival and, although a wide range of drugs targeting the different cell functions necessary for cell division are now available, resistance to chemotherapy is frequently encountered in the clinic.

One of the most commonly used chemotherapeutic agents is paclitaxel and its derivative docetaxel (a semisynthetic analogue).[1,2] These compounds target microtubules, which are essential components of the cytoskeleton, are involved in cell motility, intracellular transport, and maintenance of cell shape, and form part of the mitotic spindle that allows chromosome separation during cell division.[3,4]

In this context, the development of the multidrug-resistance (MDR) phenotype in paclitaxel-treated patients[5,6] has

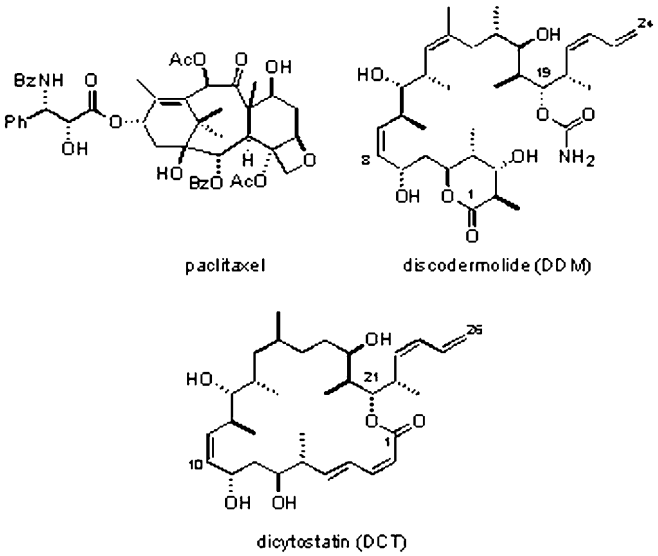


[a] Dr. A. Canales, R. Matesanz, Prof. Dr. J. M. Andreu, Dr. J. F. Díaz, Prof. Dr. J. Jiménez-Barbero
Centro de Investigaciones Biológicas, CSIC
Ramiro de Maeztu 9, 28040 Madrid (Spain)
Fax: (+34) 91-564-4853
E-mail: fer@cib.csic.es
jjbarbero@cib.csic.es

[b] N. M. Gardner, Prof. Dr. I. Paterson
Department of Chemistry, University of Cambridge
Lensfield Road, Cambridge, CB2 1EW (UK)

[**] The Bound Conformation of Microtubule-Stabilizing Agents, Part 2; for Part 1 see: J. Jiménez-Barbero, A. Canales, P. T. Northcote, R. M. Buey, J. M. Andreu, J. F. Díaz, *J. Am. Chem. Soc.* **2006**, *128*, 8757–8765.

Supporting information for this article is available on the WWW under http://www.chemeurj.org/ or from the author.

   

triggered the search for novel compounds that display the same mechanism of action but are less prone to resistance effects. Indeed, in the last 10 years, many new, structurally unrelated compounds that stabilize microtubules and mimic the activity of paclitaxel/docetaxel have been found from various sources (including corals, marine sponges, bacteria, and plants).[7–15] In a previous study,[16] these microtubule-stabilizing agents (MSA) were classified according to their binding site, either the paclitaxel-binding site or the alternative laulimalide-binding site.[14,15]

From a structural perspective, the paclitaxel-binding site, located in the lumen of the microtubules,[17] is not easily accessible to the paclitaxel molecules in solution. However, it was also shown that paclitaxel binds very quickly to microtubules[18] and that a fluorescent tag attached to paclitaxel bound to microtubules can be recognized by an antibody,[19] which indicates an additional, and external, accessible binding site. This apparent paradox of a hidden but easily accessible luminal binding site was elucidated by the discovery of a new external binding site,[20] to which a covalently binding MSA, cyclostreptin,[12,21] binds before being internalized to the luminal site.

Although paclitaxel and epothilone are known to bind to the luminal site,[17,22] detailed knowledge of where the other paclitaxel mimics bind remains elusive. Since blocking of the external site stops paclitaxel binding,[20] all the known paclitaxel-binding-site ligands should be in competition.

Among the taxoid mimetics, discodermolide (DDM),[10] originally isolated from the deep-sea sponge *Discodermia dissoluta*, displays the highest binding constant to the paclitaxel site.[16] It shows potent antiproliferative activity against a wide range of human cancer cell lines, including P-glycoprotein-overexpressing cell lines.[10,23]

Another potent taxoid mimetic is dictyostatin (DCT), originally isolated from a marine sponge of the *Spongia* genus.[24] Its binding constant for the paclitaxel site is 20 times larger than that of paclitaxel itself.[16] From a structural perspective, there are strong similarities between discodermolide and dictyostatin,[25] which suggests that their bioactive conformations may be similar. Indeed, a hybrid molecule has recently been designed on these grounds.[26]

Despite apparently binding to the same site, the existence of synergy in the effects of paclitaxel and discodermolide on cells and microtubules has been reported.[27–30] These observations could indicate binding to an additional site, such as the recently discovered pore site present in unassembled tubulin, although this is merely speculative.

In elegant recent work by Carlomagno and co-workers,[31] the unassembled-tubulin-bound conformation of discodermolide was reported. Because high-affinity taxane binding does not take place in unassembled tubulin but in assembled microtubules,[20,32] it is uncertain whether the tubulin-bound conformation described therein[31] represents the conformation bound to the luminal taxane-binding site; thus, this requires further exploration.

The knowledge of the bioactive conformation of these molecules is of paramount interest for the rational design of analogues with improved activity. Thus, in this context, we herein report the NMR investigation of the bioactive conformations of both discodermolide and dictyostatin when bound to microtubules. We compare the bound conformations with their geometries in the free state in different solvents,[33,34] as well as with the conformation of discodermolide in the presence of unassembled tubulin reported by Carlomagno and co-workers.[31]

## Experimental Section

**Protein and chemicals**: Purified calf-brain tubulin and chemicals were used as described previously.[35] Discodermolide and dictyostatin were synthesized as reported by Paterson et al.[13,36,37] The compounds were diluted in dimethylsulfoxide (DMSO) solution to give a final concentration of 10 mM and stored at −20 °C.

**Preparation of samples for the NMR experiments**: The preparation of the samples has been described already.[35] However, we repeat the basic features of the protocol for the sake of clarity. A slowly hydrolyzable nucleotide analogue, guanosine 5′-(α,β-methylenetriphosphate) (GMPCPP),[38] was employed to assemble tubulin. Guanosine 5′-triphosphate (GTP)-bound tubulin in 10 mM sodium phosphate buffer with 6 mM $MgCl_2 \cdot H_2O$ and 1 mM GTP at pH 6.7 was unable to assemble into microtubules at concentrations up to 200 μM.[32] However, when the GTP was substituted by GMPCPP and potassium in the buffer, the critical concentration is very low (4.6 μM at 37 °C). Thus, the protein was equilibrated in a buffer comprising 10 mM potassium phosphate, 6 mM magnesium chloride, and 0.1 mM GMPCPP in $D_2O$ (99.9 %, Merck) at pD 7.0 by a two-step procedure. Sucrose and GTP were removed by a drained centrifuge column of Sephadex G-25 (6×1 cm) equilibrated in a buffer consisting of 10 mM potassium phosphate and 10 μM GTP in $D_2O$ (99.9 %, Merck) at pD 7.3. This was followed by a second chromatography process in a cold Sephadex G-25 column equilibrated in 10 mM potassium phosphate in $D_2O$ (99.9 %, Merck) at pD 7.3, and then 6 mM magnesium chloride and 0.1 mM GMPCPP were added to the solution to give a pD value of 7.0. Immediately before the experiments were performed, the protein concentration was adjusted to 20 μM, the desired amount of target ligand was added to give a final 100–400 μM concentration, and the sample was incubated for 30 minutes at 298 or 310 K (depending on the temperature of the experiment). The sample was found to be completely stable for overnight experiments and only started to slowly degrade after 20 h. Under these conditions, the critical concentration of tubulin is 1.5 μM at 298 K and 0.9 μM at 310 K. This means that either 92.5 or 95.5 % of the sample (at 298 or 310 K, respectively) is assembled into microtubules. A portion of the formed polymers was adsorbed onto formvar/carbon-coated 300 mesh copper grids, negatively stained with 1 % uranyl acetate, observed with a Jeol 1230 transmission electron microscope (JEOL, Tokyo, Japan), and found to consist of microtubules.

**Computational methods**

*Conformational searching and dynamics*: Molecular mechanics calculations on DDM and DCT were performed by using the Maestro 7.5 package[39] and the MM3* force field.[40] Bulk-water solvation was simulated by using the generalized Born/surface area (GB/SA) continuum solvent model.[41] The conformational searches were carried out with 20000 steps of the usage-directed Monte Carlo/energy minimization (MC/EM) procedure. Extended nonbonded cutoff distances (a van der Waals cutoff of 8.0 Å and an electrostatic cutoff of 20.0 Å) were used.

For the Monte Carlo/stochastic dynamics (MC/SD) simulations, van der Waals and electrostatic cutoffs of 25 Å, together with a hydrogen-bond cutoff of 15 Å, were used. The dynamic simulations were run by using the MM3* force field. Charges were taken from the force field. The same degrees of freedom of the MC/EM searches were used in the MC/SD runs. All simulations were performed at 300 K, with a dynamic time step of 1 fs and a frictional coefficient of 0.1 $ps^{-1}$. Two runs of 10 ns each were performed by starting from the major conformations of the substrates, se-

  

lected from the MC/EM outputs. The Monte Carlo acceptance ratio was about 2%; each accepted MC step was followed by an SD step. Structures were sampled every 1 ps and saved for later evaluation. Monitoring of both energetic and geometrical parameters checked the convergence.

*Molecular dynamics simulations and docking calculations*: Docking of discodermolide and dictyostatin was performed by using the AutoDock 3.0 program.[42] During an AutoDock 3.0 simulation, multiple Lamarckian genetic algorithm runs occurred, with each one providing a predicted binding mode, and cluster analysis was performed at the end of the simulation. Atomic coordinates for the different conformers were obtained from molecular mechanics calculations (see above). The α/β-tubulin dimer coordinates (PDB code 1JFF)[43] were taken from the Protein Data Bank[44] and used as described.[35]

Grids of probe-atom interaction energies and electrostatic potentials were generated by the AutoGrid program present in the AutoDock 3.0 package. Grid spacings of 0.6 and 0.375 Å were used for the global and local searches, respectively. For each calculation, 1 job of 100 docking runs was performed by using a population of 200 individuals and an energy evaluation number of $3\times10^6$.

**NMR experiments**: NMR spectra were recorded at 298–313 K in $D_2O$ on Bruker AVANCE 500 and 700 MHz spectrometers. For the experiments with the free ligands, the compounds were dissolved in $D_2O$ and argon was passed through to degas the solution. TOCSY[45] and HSQC[46] experiments were performed by using the standard sequences. 2D transverse-ROESY (T-ROESY) experiments[47] were performed with mixing times of 300, 400, 500, and 600 ms. The 500 MHz NOESY[48] cross-peaks were basically zero at room temperature and moderately positive at 313 K. The strength of the 180° pulses during the T-ROESY spin-lock period was attenuated four times with respect to that of the 90° hard pulses (between 7.2 and 7.5 μs). To deduce the interproton distances, relaxation-matrix calculations were performed by using software written in house, which is available from the authors upon request.[49]

For the bound ligands, TR-NOE experiments were performed as previously described with a freshly prepared ligand/microtubule solution.[35] TR-NOESY experiments were then performed with mixing times of 50, 100, 200, 250, and 300 ms, for molar ratios of ligand/protein from 5:1 to 20:1. No purging spin-lock period to remove the NMR signals of the macromolecule background was employed, since they were basically not observable due to the huge size of the receptor. First, line broadening of the ligand protons was monitored after addition of the ligand. Strong negative NOE cross-peaks were observed, in contrast to the results for ligands in the free state; these cross-peaks indicated binding of both molecules to the microtubule preparation. The theoretical analysis of the TR-NOEs of the ligand protons was performed according to the CORCEMA program[50,51] by using a relaxation matrix with exchange, as previously described.[35] Different exchange-rate constants were employed to obtain the optimal match between the experimental and theoretical results of the intraresidue cross-peaks of the protons belonging to the *Z* double bonds of discodermolide (H8, H9) and dictyostatin (H10, H11), which have a relatively fixed geometry for any given protein/ligand ratio. The overall correlation time, $\tau_c$, for the free state was always set to 0.35 ns, since NOESY cross-peaks for the free molecule were basically zero at room temperature and 500 MHz. The $\tau_c$ value for the bound state was set to 100 ns. To fit the experimental TR-NOE intensities, off-rate constants, $k_{off}$, between 50 and 500 $s^{-1}$ were tested. Optimal agreement was achieved for $k_{off}=150\ s^{-1}$.

T-ROESY experiments were also carried out to exclude spin-diffusion effects. A continuous-wave spin-lock pulse was used during the 250 ms mixing time. Key NOEs were shown to be direct cross-peaks, since they showed different signs to the diagonal peaks.[52,53]

## Results and Discussion

**The conformation of free discodermolide in water solution**: The conformational behavior of free discodermolide in the unbound state has been previously explored both in the solid state and in two different solvents, DMSO and acetonitrile.[33,34] The conclusions are strikingly different. Discodermolide in DMSO seems to be a very flexible molecule with over ten conformers contributing to the conformational equilibrium.[34] Curiously, the form observed by X-ray crystallography is claimed to represent less than 1% of the population in this solvent. By contrast, the major conformation deduced in acetonitrile solution,[33] which arises from minimization of $A^{1,3}$ strain and *syn*-pentane nonbonded interactions, was in good agreement with the solid-state conformation, except for the orientation of the δ-lactone. Subtle differences in the overall shape of the six-membered lactone ring were also evident in the three studies. In principle, two types of conformers were proposed: the chair conformer with two axially and equatorially oriented substituents, somewhat distorted towards a $^3H_4$ half-chair form (in acetonitrile, in the solid state, and partially in DMSO), or a $^3S_1$ skew-boat form. The different possibilities, along with their structural features, are given in Tables 1 and 2, and Table S3 and Figures S1, and S11 in the Supporting Information.

In this work, the conformation of discodermolide in water solution ($D_2O$) was explored. The 500 MHz NOESY cross-peaks were basically zero at room temperature and moderately positive at 313 K. Thus, T-ROESY experiments were used to access the key conformational information. A complete assignment of the $^1H$ NMR resonance signals of discodermolide was achieved on the basis of TOCSY, HSQC, and T-ROESY experiments. The difference in chemical shifts and coupling constants (Figure S11 in the Supporting Information) between the reported data in acetonitrile and those measured in water are given in Table S1 in the Supporting Information. Some noticeable differences are observed for the chemical shifts, which are similar for the H12 to H16 region, including the corresponding methyl groups, and rather different for the other parts of the molecule, especially for the lactone moiety and from C17 to the C24 tail.

The analysis of the vicinal proton–proton coupling constants for the six-membered ring permitted its conformation to be assessed. Generally speaking, no major changes were deduced for the coupling constants between the available dimethylsulfoxide and acetonitrile values and those recorded in water. A clear difference is only observed for the $^3J_{H4,H5}$ coupling between water and DMSO on the one hand and acetonitrile on the other, but this is likely to be a typographic mistake in the latter publication.

To assess the conformational distribution in water, the *J* data were complemented by NOE experiments. The relationship between NOE signals and proton–proton distances is well established and can be worked out at least semiquantitatively by using a full relaxation-matrix approach.[54] The NOE intensities reflect the conformer populations, and therefore information on the population distributions in free solution can be obtained by focusing on the key NOEs that characterize the different possible conformations.

At 500 MHz and room temperature, all of the cross-peaks observed in the NOE spectra of discodermolide in water so-

  

Table 1. Analysis of the estimated interproton distances for discodermolide in the free and tubulin-bound states. For the bound state, the experimental distances, $r$ [Å], are estimated according to a full matrix-relaxation approach from a CORCEMA-based[46] analysis of the TR-NOESY data. The H8–H9 and H21–H22 distances (2.2 Å) were taken as internal references. The estimated experimental errors are considered to be around ±10%. The reported data for the free state in acetonitrile[31] or dimethylsulfoxide[32] are also given. The best fits between our data in the free state and those reported in references [31] or [32] are underlined. Key NOEs that further support this conclusion are in bold.

| Proton pair | Predicted for the major conformer in the skew form (MM3*) | Predicted for the major conformer in the half-chair form (MM3*) | Reported for the free state in $CD_3CN$[a] | Reported for the free state in DMSO[b] | From the experiment: T-ROESY build up curve for the free state (error: ±10%) | From the experiment: NOESY build up curve for the bound state (error: ±10%) |
|---|---|---|---|---|---|---|
| H2–H3 | 2.9 | 2.6 | 2.6 | – | 2.8 | 2.6 |
| H2–H5 | 2.8 | 4.1 | 4.1 | 2.6 | 3.4 | >3.7 |
| H3–H4 | 2.4 | 2.4 | 2.5 | 2.3 | 2.5 | 2.5 |
| H3–$CH_3$25 | 2.5 | 2.4 | 3.0 | 3.1 | 2.4 | 2.4 |
| H3–$CH_3$26 | 2.7 | 2.0 | 3.1 | 3.1 | 2.5 | 2.2 |
| H4–H18 | 2.8 | 2.8 | – | – | 2.8 | 2.8 |
| H4–$CH_3$25 | 3.7 | 2.4 | 2.8 | – | 2.8 | 2.5 |
| H5–H7 | 3.1 | 3.1 | 3.2 | 3.4 | overlap | overlap |
| H5–$CH_3$26 | 2.7 | 2.5 | 3.1 | 3.1 | 2.6 | 2.5 |
| H6R–H8 | 3.0 | 3.0 | 3.1 | – | 2.7 | 3.1 |
| H6R–H15 | 2.1 | 2.3 | – | – | 2.3 | 2.3 |
| H6S–$CH_3$26 | 2.3 | 2.2 | 2.7 | -- | 2.2 | 2.2 |
| H7–H9 | 3.7 | 3.6 | **3.8** | 2.4 | not observed | not observed |
| H7–H10 | 2.1 | 2.2 | 2.1 | 2.2 | 2.0 | 2.3 |
| H7–$CH_3$27 | 3.0 | 2.8 | 3.2 | 3.4 | 2.8 | 2.9 |
| H8–H12 | 4.0 | 3.6 | **4.2** | 2.9 | not observed | not observed |
| H8–H22 | 2.9 | 2.7 | – | – | 2.7 | 2.8 |
| H9–H11 | 3.7 | 3.6 | **3.8** | 2.7 | not observed | not observed |
| H9–H12 | 2.8 | 2.8 | 2.9 | 2.8 | 2.6 | 2.9 |
| H10–H11 | 2.5 | 2.3 | 2.5 | – | 2.3 | 2.4 |
| H10–H13 | 2.8 | 2.9 | 3.0 | 2.8 | 2.8 | 2.9 |
| H10–$CH_3$27 | 2.5 | 2.4 | 2.9 | – | 2.4 | 2.4 |
| H11–H12 | 3.1 | 2.9 | 3.1 | 3.0 | 3.1 | 3.0 |
| H11–H13 | 2.5 | 2.4 | 2.4 | 2.4 | 2.3 | 2.5 |
| H11–$CH_3$27 | 2.5 | 2.4 | 3.0 | 3.0 | 2.4 | 2.4 |
| H11–$CH_3$28 | 2.6 | 2.6 | 3.2 | 3.1 | 2.5 | 2.5 |
| H12–H15R | 2.0 | 2.1 | 2.0 | 2.2 | 2.0 | 2.1 |
| H12–$CH_3$30 | 3.4 | 3.3 | **3.7** | 4.3 | **3.2** | 3.2 |
| H13–$CH_3$28 | 2.8 | 2.7 | 3.2 | 3.1 | 2.6 | 2.6 |
| H15B–$CH_3$31 | 2.7 | 2.7 | 3.2 | – | 2.6 | 2.6 |
| H16–$CH_3$29 | 2.4 | 2.3 | – | – | 2.2 | 2.4 |
| H16–$CH_3$31 | 2.2 | 2.2 | – | – | 2.0 | 2.3 |
| H17–H18 | 2.5 | 2.3 | 2.5 | 2.3 | 2.4 | 2.4 |
| H17–H19 | 3.1 | 2.9 | 3.1 | 2.9 | 3.0 | 3.0 |
| H17–H20 | 2.1 | 2.1 | 2.1 | – | 2.1 | 2.3 |
| H17–H23 | 2.4 | 2.5 | 2.5 | 2.5 | 2.5 | 2.6 |
| H17–$CH_3$30 | 2.5 | 2.5 | 3.0 | 2.6 | 2.5 | 2.5 |
| H18–H21 | 2.9 | 2.9 | 2.7 | 2.6 | 2.8 | 3.0 |
| H18–H20 | 3.1 | 3.1 | – | – | 3.0 | 3.1 |
| H18–H19 | 3.1 | 2.9 | 3.1 | – | 2.9 | 2.8 |
| H18–H21 | 2.9 | 2.9 | – | – | 2.9 | 2.9 |
| H19–H20 | 2.5 | 2.4 | 2.4 | – | 2.4 | 2.4 |
| H19–H21 | 3.8 | 3.7 | – | 3.0 | not observed | not observed |
| H19–$CH_3$31 | 2.6 | 2.6 | **2.6** | 3.1 | **2.6** | 2.6 |
| H19–$CH_3$32 | 2.5 | 2.5 | **2.5** | 2.9 | **2.5** | 2.5 |
| H20–H21 | 3.1 | 3.1 | – | – | 3.1 | 3.1 |
| H20–H23 | 2.1 | 2.1 | 2.1 | 2.2 | 2.1 | 2.2 |
| H21–$CH_3$32 | 2.6 | 2.6 | 3.3 | 3.0 | 2.6 | 2.5 |
| H22–H24 | 2.5 | 2.5 | 2.5 | 2.2 | 2.4 | 2.5 |

[a] See reference [31]. [b] See reference [32].

lution were very weak, almost close to zero. The $\omega\tau_c$ value is close to 1.1 and provides an almost zero longitudinal NOE.[54] Thus, the basic information was derived from T-ROESY experiments,[47] which provided the crucial cross-peaks that are reported in Table 1. The spectrum is shown in Figure S2 in the Supporting Information. By comparing these NOE parameters, it could be deduced (see Table 1) that the observed values in water are more similar to those available in acetonitrile than to those reported in DMSO.

Table 2. Comparison between the experimental values of *J* couplings in water solution (this work) and those reported for discodermolide in dimethylsulfoxide and acetonitrile solutions.[31,32] The two values between brackets in the *J* exp water column correspond to the expected values for the skew-boat and chair conformers, respectively. The couplings for the six-membered ring are in agreement with a percentage of skew boat of around 60–75%. The couplings for the lateral chains are in agreement with a major conformation for most of the linkages (see percentages). For each linkage, the major conformer is given.

| Torsion angle | *J* exp DMSO[a] | *J* exp MeCN[b] | *J* exp $H_2O$ (this work) | Estimated chair/skewboat equilibrium | Estimated % of a major conformer around the corresponding linkage |
|---|---|---|---|---|---|
| H2–H3 | not reported | 4.2 | 3.6 (1.2, 5.2) | 40:60 | |
| H3–H4 | not reported | 4.2 | 3.5 (1.2, 4.2) | 25:75 | |
| H4–H5 | 10 | 2* (typographic mistake) | 10.1 (10.7, 10.2) | | |
| H5–H6*S* | <1 | <1 | 1.8 | | >90 |
| H5–H6*R* | 10 | 10.0 | 9.5 | | >80 (*anti* type) |
| H6*S*–H7 | 9.5 | 10.8 | 9.9 | | >85 (*anti* type) |
| H6*R*–H7 | <1 | 2.4 | 1.8 | | >90 |
| H7–H8 | 9.5 | 9.1 | 9.0 | | >80 (*anti* type) |
| H9–H10 | 10 | 10.1 | 10.5 | | >95 (*anti* type) |
| H10–H11 | 2.2 | not given | 2.4 | | >85 (*syn* type) |
| H11–H12 | 8.8 | 6.6 | 9.8 | | >90 (*anti* type) |
| H12–H13 | 10 | 10.0 | 10.1 | | >95 (*anti* type) |
| H16–H17 | 7.8 | 6.2 | 7.3 | | >60 (equilibrium) |
| H17–H18 | 2.3 | 3.5 | 2.8 | | >80 (*syn* type) |
| H18–H19 | 9.1 | 8.0 | 9.5 | | >90 (*anti* type) |
| H19–H20 | 2.8 | 4.1 | 3.4 | | >80 (*syn* type) |
| H20–H21 | 10 | 10.6 | 10.7 | | >95 (*anti* type) |
| H22–H23 | not reported | 10.7 | 11.3 | | >95 (*anti* type) |

[a] See reference [32]. [b] See reference [31].

The conformation of the six-membered lactone ring was first addressed. The coupling constants (Table 2a) are in between those expected for the half chair and the skew boat.

With regard to the NOE values (Table 1), the key H2–H3 NOE (corresponding distance 2.8 Å) is always (at all mixing times) significantly weaker than the H3–H4 NOE (2.5 Å). This fact, together with the observation of a weak H2–H5 cross-peak, is in agreement with the presence of a certain population of the skew-boat form (Table 1). The stronger H3–$CH_3$25 NOE (medium, 2.4 Å) with respect to that of H3–$CH_3$26 (medium, 2.5 Å) also supports the existence of an equilibrium between the $^3S_1$ skew-boat form and the half-chair conformer. The energy difference between both forms is indeed small (less than 2 kcal mol$^{-1}$) according to MM3* calculations, and this supports the existence of both geometries in solution.

For the rest of the molecule, close inspection of the *J* values indicates the presence of conformational averaging, especially around C16–C17 ($J_{H16,H17}$ = 7.3 Hz). No *J* information is available for the C14–C15 fragment. For most of the C–C linkages, the vicinal H–H couplings are either equal or larger than 9 Hz or smaller than 3.5 Hz, thereby indicating the presence of a major geometry around the different linkages (>85%), especially around C9–C10, C12–C13, C20–C21, and C22–C23 (*J* = 10 Hz or larger, with more than 90% for a given geometry). Values of around 9.0–9.8 Hz are observed for the C5–C6, C6–C7, C7–C8, C11–C12, and C18–C19 bonds. Therefore, a major conformation is also present for these linkages (80–90%), although minor contributions from alternative orientations are possibly taking place. Different geometries for rotation around these linkages are given in the Supporting Information.

Nevertheless, the global minimum found in the MM3* calculations provides the best fit between the expected and observed NMR spectroscopic data. This conformation, with skew-boat geometry for the lactone ring, is depicted in Figure 1. Additional possible conformations found around the C11–C12, C16–C17, and C18–C19 linkages are depicted in Figure S3 in the Supporting Information.

There are several NOEs that define the topology of the chain. As mentioned before, no couplings are available for the C14–C15 linkage. However, the H12–H15R and the $CH_3$28–$CH_3$30 NOEs are sensitive to the corresponding C12–C13, C14–C15, and C15–C16

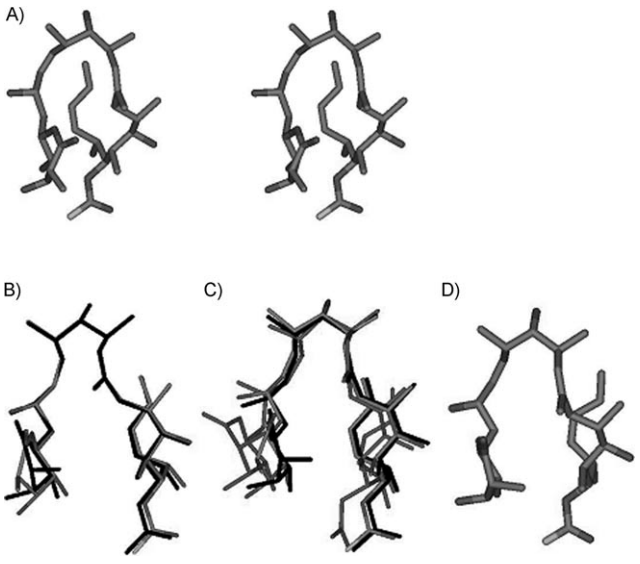


Figure 1. Conformation analysis of discodermolide. A) Stereoscopic view of the global minimum of DDM in water solution. B) Superimposition of the half-chair and skew-boat conformers of discodermolide showing the major conformer around the C5–C24 chain. C) Superimposition of these two forms with that deduced by Carlomagno and co-workers for DDM bound to soluble tubulin.[31] Some differences in the orientation and shape of the six-membered ring can be appreciated. D) The bound conformer to assembled microtubules, as deduced by TR-NOESY experiments (see text).

  

torsions. The average experimental H12–H15R distance is 2.1 Å, whereas the $CH_3$28–$CH_3$30 distance is around 2.6 Å; these results indicate a very major conformation (close to the MM3* global minimum) in this region. Moreover, the H4–$CH_3$31 (2.8 Å) and H8–H22 NOEs (2.7 Å) indicate a major orientation between the six-membered ring and the C13–C19 side chain and between the C5–C13 and C19–C22 side chains, respectively, in agreement with the predicted MM3* global minimum (Figure S9 in the Supporting Information). Nevertheless, some of the expected NOEs for short to moderate distances are missing, thereby indicating the presence of conformational averaging. With all of these *J* and NOE data simultaneously observed, it can be safely assumed that, although there is a major global conformation in water solution, there is conformational heterogeneity especially at the lactone moiety and at the C16–C17 linkage. The fact that there is conformational mobility is evident by the lack of the H21–$CH_3$26 NOE, which is at a relatively short distance for both the skew (2.6 Å) and the chair (2.9 Å) forms, and of the H12–H24 NOE (at a moderate distance of 3.1–3.2 Å). Nevertheless, the conformational rigidity of discodermolide in water is significantly higher than in the organic solvents previously studied.[33,34] The hairpinlike shape of the molecule in its major conformation (Figure S9 in the Supporting Information) makes possible the presentation of all of its polar groups at the periphery, thus favoring their interaction with the solvent molecules and minimizing the lipophilic surface for interaction with water.

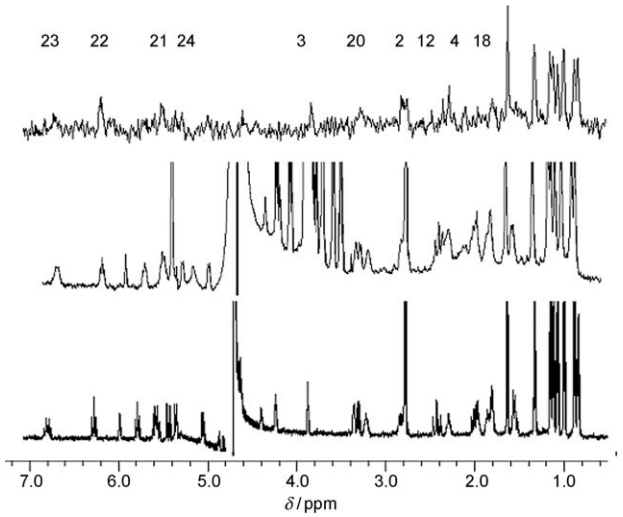


Figure 2. $^1$H NMR spectra (500 MHz) of DDM in water solution with different experimental conditions at 298 K. Bottom trace: DDM in the free state. Middle trace: DDM in the presence of microtubules ($D_2O$, 298 K), with a DDM/tubulin molar ratio of 20:1. The large signals of the nucleotide employed to stabilize the microtubules are evident. Top trace: STD spectrum (saturation time: 2 s) of DDM in the presence of microtubules, with a DDM/tubulin molar ratio of 20:1. Apart from the methyl groups, which show clear intensities, the most significant STD signals are marked with the number of the corresponding proton resonances. The signals of the nucleotide do not appear in the STD spectrum (huge nucleotide/tubulin ratio).

### NMR TR-NOESY studies of discodermolide and dictyostatin in the presence of microtubules

*Discodermolide*: The key point in trying to understand the properties of DDM is to deduce the bioactive conformation bound to microtubules.[55] As previously shown, for ligands that are not bound tightly and that exchange between the free and bound states at a reasonably fast rate, the transferred nuclear Overhauser enhancement spectroscopy experiment (TR-NOESY) provides an adequate means to determine the conformation of the bound ligand.[35,56] As previously described,[35] and to work with biochemical conditions in which microtubules are stable, native tubulin was assembled with GMPCPP (see reference [35] and also the Experimental Section).

The addition of the microtubule solution to an NMR tube containing discodermolide induced broadening of the resonance signals in the $^1$H NMR spectrum, which indicates that binding occurs (Figure 2).

TR-NOESY experiments (Figure 3 and Figures S4 and S7 in the Supporting Information) were then performed on the ligand/microtubule sample at different mixing times. Negative cross-peaks were clearly observed at 303 K, as expected for ligand binding and in contrast with the observations for the free ligand, for which no NOEs were observed (zero crossing in the NOE curve).

For the 10:1 to 20:1 ligand/protein molar ratios employed, obviously the coupling constants are basically defined by the couplings in the free state, thus the bound geometry has to be defined by the TR-NOE data. The observed NOE data for the bound state are very similar to those described above for discodermolide in water. Now, however, the NOE data are in agreement with a half-chair conformation for the

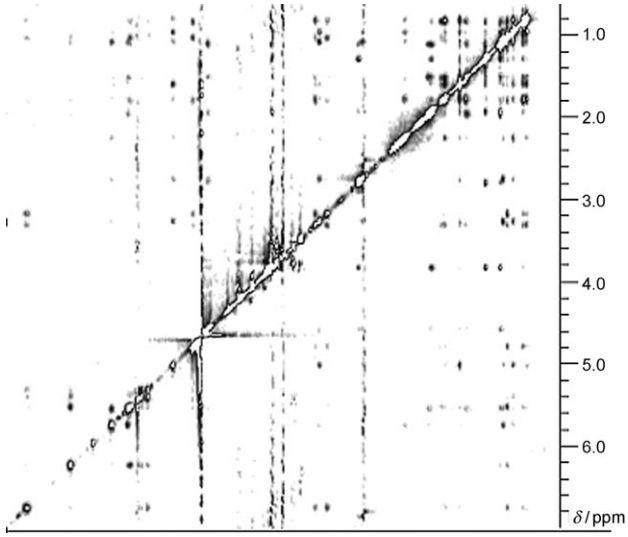


Figure 3. TR-NOESY spectrum (mixing time: 100 ms) of discodermolide (DDM) in the presence of microtubules ($D_2O$, 298 K), with a tubulin/DDM molar ratio of 20:1. Negative cross-peaks are observed, which indicates that the bioactive conformation can be extracted from the quantitative analysis of these peaks.

  

six-membered ring orientation, due to the weakness of the H2–H5 cross-peak, as well as the relative changes in the intensities of the key NOEs from the $CH_3$25 and $CH_3$26 signals. Thus, there is a conformational selection process regarding the shape of the six-membered ring. Nevertheless, despite this conformational selection for the lactone ring, the orientation of the six-membered ring moiety relative to the backbone is almost identical to that observed in the free state, as shown by the key short contacts mentioned above (Table 1). Also, the analysis of the TR-NOESY cross-peaks, by using a full relaxation-matrix approach, with the help of the CORCEMA program, permitted us to deduce that the relative orientation of the C5–C24 hydrocarbon chain remains basically unaltered upon binding.

T-ROESY experiments allowed the exclusion of spin-diffusion effects for the key cross-peaks. Thus, the observed pattern is that expected for a conformer with no significant distortion by the microtubules in the area of C5–C24 from the global shape of the major conformer deduced in water. On the other hand, the observed cross-peaks are in agreement with the existence of a conformational selection process for the lactone. Therefore, while distinct flexibility appears for the different torsional degrees of freedom of discodermolide in acetonitrile or dimethylsulfoxide,[33,34] the orientation of the C5–C24 chain is highly preorganized in water solution with respect to that bound by tubulin, probably to minimize entropic penalties. A preorganized conformation of discodermolide in water solution is supported by a favorable entropy change upon its binding to microtubules of 80 $J\,mol^{-1}\,K^{-1}$, which is reduced to 10 $J\,mol^{-1}\,K^{-1}$ in DCT (see below) and which changes sign for other MSAs (taxanes and epothilones).[18] Views of the polar and nonpolar surfaces of the major conformer are shown in Figure 4.

There are some slight changes in the deduced bound conformation with respect to that described by Carlomagno and co-workers with unassembled tubulin.[31] A superimposition is shown in Figure 1. Although the structure provided by Carlomagno and co-workers[31] shows a chair for the six-membered ring and its orientation is somewhat different with respect to the rest of the chain, the presentation of the molecule is remarkably similar, despite the change in the mode of preparation of tubulin in both cases.

Further insights into the mode of binding of DDM were deduced from saturation transfer difference (STD) experiments.[57] First, the interaction was demonstrated to be specific by using competitive STD experiments.[58] Thus, baccatin, the core skeleton of paclitaxel and docetaxel, was employed as a model ligand. Baccatin binds to microtubules and competes with paclitaxel, although with 100-times-lower affinity ($1.5\times10^5\,M^{-1}$ for Baccatin III as compared with $3.7\times10^7\,M^{-1}$ for paclitaxel). Clear STD (Figure 5) and TR-NOE signals were obtained for baccatin when it was added to a solution containing microtubules. The STD (Figure 5) and TR-NOE signals (data not shown) were completely removed from the corresponding spectra when discodermolide or dictyostatin were added to the same NMR tube, thus indicating that these compounds compete for the taxane-binding site in microtubules, as already described, and both have a much higher affinity than baccatin III.

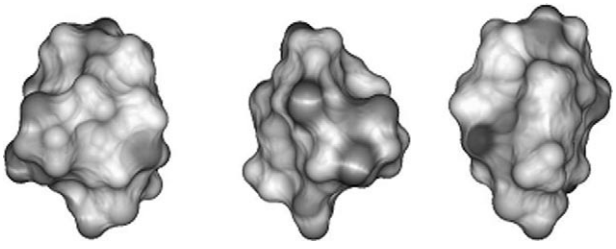

Figure 4. Different perspectives of the representation of the polar and nonpolar areas of the conformer of discodermolide bound by microtubules. This conformer seems to have a well-defined patch of polar and nonpolar areas.

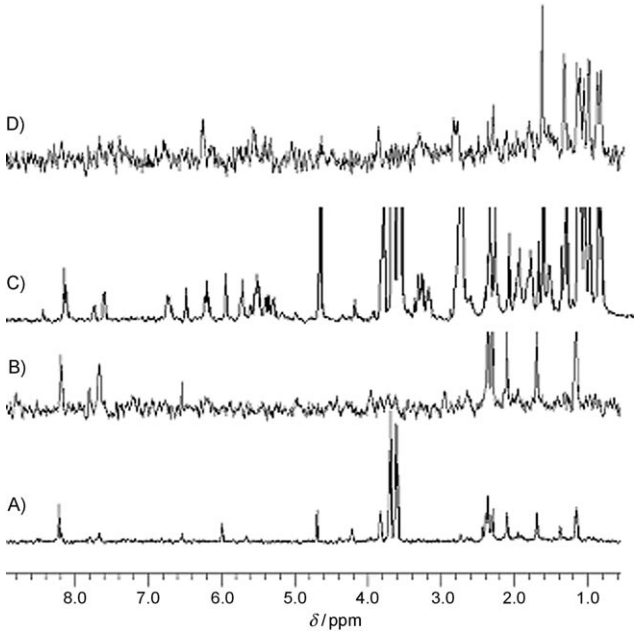


Figure 5. A) $^1$H NMR (500 MHz) spectrum of baccatin in the presence of microtubules ($D_2O$, 298 K), with a baccatin/tubulin molar ratio of 15:1. B) STD spectrum of this sample. The signals of baccatin are evident. C) $^1$H NMR spectrum of DDM and baccatin in the presence of microtubules ($D_2O$, 298 K), with a baccatin/DDM/tubulin molar ratio of 10:10:1. D) STD spectrum (saturation time: 2 s) of this last sample. The STD spectrum corresponds to that observed for DDM (Figure 2). Thus, the signals of baccatin are removed, which indicates competitive binding. Similar effects were observed when dictyostatin was added to the NMR tube containing baccatin.

Moreover, when the amount of DDM or DCT was increased, the TR-NOE spectra depicted in Figure 3 and in Figure S4 in the Supporting Information were again obtained, as well as the corresponding STD spectra for these molecules (Figure 5).

STD experiments were performed on the same TR-NOESY samples mentioned above. Although the beneficial accumulation effect of STD experiments in terms of the signal/noise ratio makes preferable the use of high ligand/receptor ratios, the limited solubility of both DDM and DCT

  

in water solution only permitted the use of the 10:1 or 20:1 molar ratio samples described above. The corresponding STD spectrum for DDM is shown in Figure 2. For discodermolide, the STD spectrum provided clear enhancements for the methyl groups at the periphery of the backbone, and for certain signals, especially those belonging to the lactone ring (H2–H4), H12, and the C18–C24 portion of the chain. Notably, H2 and H22 gave the most significant STD enhancements. The STD pattern was semiquantitatively explained by means of the CORCEMA-STD[50,51] program by using the docked structure of DDM in the tubulin-binding site (see below). A fair agreement was obtained between the experimental and modeled STD data, with an *R* factor of 0.14, more than reasonable for this molecular system.

*Dictyostatin*: As mentioned in the introduction, dictyostatin is a microtubule-stabilizing macrolide that is structurally related to discodermolide. Indeed, the configurations of the stereocenters of both molecules are remarkably homologous and consistent with a common biogenesis.[25] The conformational behavior of this molecule has been elucidated in methanol solution by using NMR spectroscopy and molecular mechanics calculations.[25] This analysis indicated the presence of an equilibrium between two major forms (Figure 6), the s-*trans* (major) and the s-*cis* (minor) forms, which basically differ in the conformation around C1–C2. The characteristic torsion angles for both forms are given in Table S3 in the Supporting Information, whereas the corresponding short distances, which can be correlated with experimental NOEs, are gathered in Table 3. The observed *J* couplings in methanol[25] were basically identical to those deduced in water solution (see Figure S5 in the Supporting Information) and, thus, indicate a similar conformational behavior in both polar solvents (see Table S2 and Figure S10 in the Supporting Information).

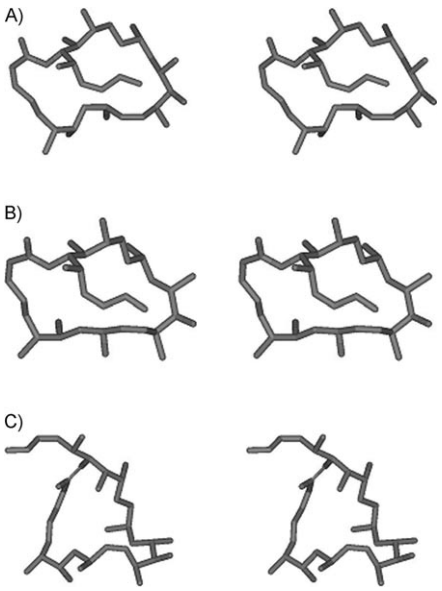


Figure 6. Conformation analysis of dictyostatin. A) Stereoscopic view of the s-*trans* global minimum. B) Stereoscopic view of the bound conformer. C) Stereoscopic view of the s-*cis* local minimum.

The bioactive conformation of DCT bound to microtubules was deduced by using TR-NOESY experiments and by following the protocol described above for DDM (see Figures S6 and S8 in the Supporting Information). Also in this case, strong negative cross-peaks were observed at 303 K, as expected for ligand binding (Figure 7). For DCT,

Table 3. Analysis of the estimated interproton distances for dictyostatin in the microtubule-bound state. The experimental distances, *r* [Å] (± 10%), are estimated according to a full matrix-relaxation approach from a CORCEMA-based analysis of the TR-NOESY data. The H10–H11 and H21–H22 distances were taken as internal references. The reported data for the free-state conformations (regular s-*trans* and s-*cis* conformers) are also given. The best-fit conformer is a secondary minimum (approximately 4.5 Kcal mol$^{-1}$) deduced from the MM3* calculations for dictyostatin. This minimum displays an s-*trans* geometry. Also, it is necessary to consider different rotamers around C20–C21 to quantitatively explain all of the NOEs involving the lateral chain. The data supporting these conclusions are in bold.

| Proton pair | Global minimum of s-*trans* [Å] | Local minimum of s-*cis* [Å] C22−C26 | Bound conformer [Å] of C22−C26[a] | Distance from experiment [Å] (error: ±10%) |
|---|---|---|---|---|
| H2–H3 | 2.4 | 2.4 | 2.3 | 2.3 |
| H2–H4 | 3.9 | 3.9 | 3.9 | **>3.5** |
| H3–H4 | 3.1 | 3.1 | 3.1 | 3.1 |
| H3–H5 | 2.6 | 2.5 | 2.5 | 2.5 |
| H4–H5 | 3.1 | 3.1 | 3.1 | 3.1 |
| H4–H6 | 2.3 | 2.3 | 2.4 | 2.4 |
| **H4–H8b** | 3.4 | 2.8 | 3.1 | 3.2 |
| H4–H23 | **2.4** | **8.4, 3.0, 6.6** | 2.6**, 4.2, 7.8** | **>3.5** |
| **H4–Me20** | 3.1 | 3.5 | 3.6 | 2.9 |
| H4–Me22 | **2.8** | **6.7, 6.1, 3.2** | **3.8, 2.6,** 7.0 | **3.4** |
| **H5–H6** | 3.1 | 3.1 | 3.1 | 3.1 |
| **H5–H7** | 3.7 | 3.9 | 3.8 | 3.5 |
| **H5–H8a** | 2.9 | 3.2 | 3.7 | 3.4 |
| **H6–H7** | 2.4 | 2.4 | 2.6 | 2.5 |
| H6–H8b | 2.5 | 2.5 | 2.8 | 2.7 |
| **H7–H10** | **2.3** | **4.6** | **4.4** | **>3.5** |
| H8b–H10 | 2.5 | 2.7 | 2.7 | 2.7 |
| **H8b–H24** | **2.7** | **8.0, 4.5, 8.7** | **3.1, 6.0, 7.0** | **3.5** |
| H10–H11 | 2.3 | 2.3 | 2.3 | 2.3 |
| **H10–H24** | **2.6** | **8.9, 5.1, 8.0** | **2.3, 4.7, 7.0** | **>3.5** |
| H11–H13 | 3.8 | 3.8 | 3.8 | 3.5 |
| **H11–H14** | **3.1** | **2.5** | **2.5** | **2.6** |
| H12–H13 | 2.5 | 2.4 | 2.4 | **2.5** |
| H12–H15a | 2.1 | 2.3 | 2.1 | 2.3 |
| **H17b–H20** | **2.3** | **4.7** | **3.1** | **3.4** |
| H19–H20 | 2.5 | 2.3 | 2.4 | 2.4 |
| H19–H21 | 3.3 | 3.6 | 3.2 | 3.3 |
| H19–H22 | 2.1 | 5.0, 4.9, 5.6 | 2.2, 3.9, 3.0 | 2.4 |
| **H19–H25** | **2.4** | **7.1, 6.6, 7.5** | **2.5, 5.0, 5.0** | **2.8** |
| H20–H21 | 3.0 | 2.3 | 3.1 | 2.6 |
| **H20–H23** | 3.1 | 4.6, 4.0, 5.4 | **3.0**, 5.3, 4.8 | 3.2 |
| H21–H22 | 2.4 | 3.1, 2.5, 2.5 | 3.1, 2.5, 2.5 | 2.7 |
| H21–H23 | 2.9 | 2.5, 3.7, 2.9 | 3.8, 4.4, 2.6 | 2.8 |
| H22–H24 | 3.8 | 3.8 | 3.8 | >3.5 |
| H22–H25 | 2.1 | 2.1 | 2.1 | 2.1 |
| H24–H25 | 3.2 | 3.2 | 3.2 | 3.2 |
| H24–H26a | 3.8 | 3.8 | 3.8 | >3.5 |
| H24–H26b | 2.5 | 2.5 | 2.5 | 2.4 |

[a] Rotamers: H21/H22 171, −60, 60.

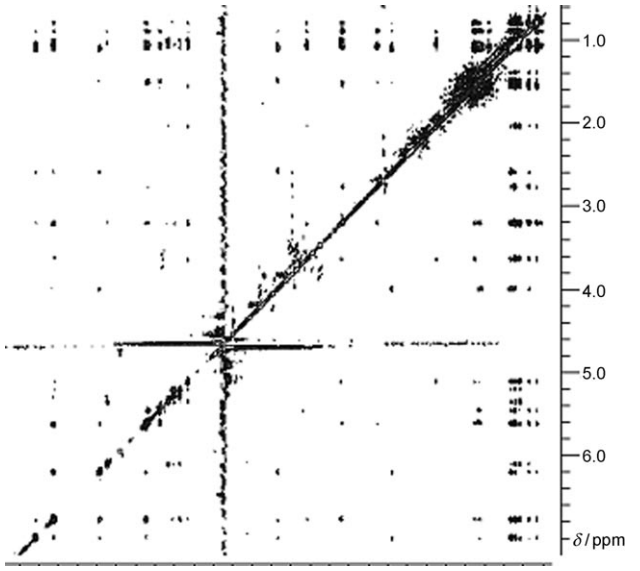


Figure 7. TR-NOESY spectrum (mixing time: 100 ms) of dictyostatin in the presence of microtubules ($D_2O$, 298 K), from which the bioactive conformation of the macrocycle is deduced. Other experiments were recorded with mixing times of 50, 150, and 200 ms.

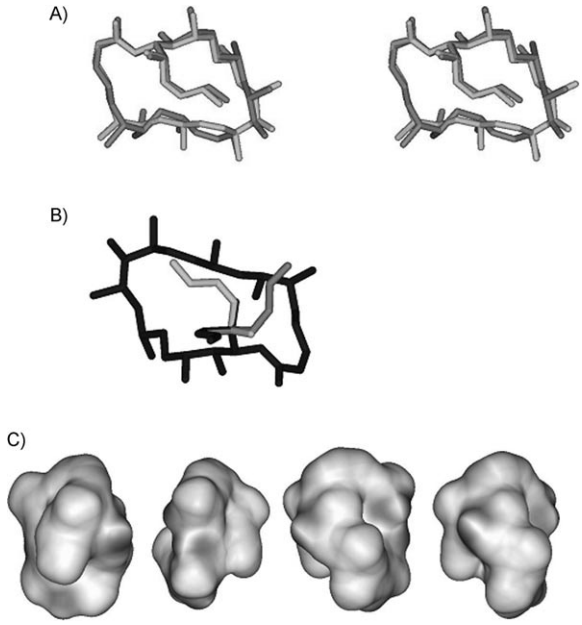


Figure 8. Conformation analysis of dictyostatin when bound to microtubules. A) Stereoscopic view of the superimposition of the major conformer found in free solution (light print) with that bound (dark print) to microtubules. The major changes affect the C8–C9 torsion angle and the corresponding adjustments. B) Superimposition of the three possible rotamers around the lateral C21–C22 linkage. C) Different perspectives of the polar and nonpolar patches of the bound conformer of dictyostatin.

no NOEs were observed in the free state (zero crossing in the NOE curve).

The observed TR-NOE cross-peaks (Figure 7 and Table 3, and Figure S8 in the Supporting Information) were translated into distances with the assistance of the CORCEMA program[50] by using the two more stable s-*cis* and s-*trans* geometries. Upon comparison of the experimental and expected values for both conformers, in this case, and contrary to the observations for DDM, no simultaneous fitting of all the NOE data could be obtained by using either individual conformer. For instance, the estimated experimental long distances for the H7–H10 and H17–H20 proton pairs (lack of these key NOEs, bold in Table 3), which are at very short distances in the regular s-*trans* geometry, together with the observation of relatively short distances for the H11–H14 and H4–$CH_3$20 pairs, clearly indicate that the global minimum, the s-*trans* form, is not bound to the microtubules (Table 3).

On the other hand, the s-*cis* geometry also fails to describe some of the observed NOEs, especially those involving the C22–C26 tail. A rotation around the C21–C22 bond, maintaining the *s-cis* form, still does not permit an explanation of the above-mentioned experimental NOEs, which are underlined in Table 3.

Thus, there is a significant conformational change in the DCT conformation upon binding to microtubules. By using the MM3*-based calculated secondary minima for DCT, the best agreement was found when a third local minimum was considered (see Table 3). This conformer displays similar torsion angles to the s-*trans* form but shows a major torsional change around the C8–C9 linkage, and minor adjustments around the entire skeleton (Figure 8). According to the MM3* calculations, the energy difference between the s-*trans* conformer and this conformer amounts to 4.7 kcal mol$^{-1}$. In addition, to fit the NOEs for the lateral diene chain, consideration of an equilibrium between at least two (probably three) rotamers around C21–C22 should be considered (Figure 8). Thus, now, it is possible to fit almost quantitatively all of the observed NOEs. Hence, there is a conformational variation process regarding the shape of the macrolide ring. Therefore, whereas DDM seems to show a preorganized conformation in water solution to interact with microtubules, this is not the case for DCT. Views of the polar and nonpolar surfaces of the bound DCT conformer are also shown in Figure 8.

The bound conformer of DCT resembles that of bound DDM (Figure 9). In fact, they display similar polar and nonpolar surfaces that allow them to interact with the corresponding receptor. Modification of the orientation of the lateral diene chain of DCT does not substantially modify the good match between both molecules.

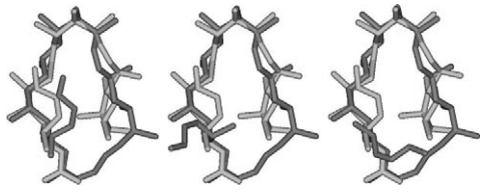

Figure 9. Superimposition of the bound conformer of discodermolide (light print) with the three possible rotamers around the lateral C21–C22 linkage of the bound conformer of dictyostatin (dark print). The degree of adjustment is more than satisfactory.

  

STD experiments were also performed on the sample of DCT in the presence of assembled microtubules (Figure 10). The experiment indicated the existence of ligand binding to the microtubules, with most of the $^1$H NMR spectroscopic signals providing clear STD enhancements, although with different intensities. The obtained enhancements and the bound conformation docked into tubulin (see below) were considered for the simulation of the STD data with the CORCEMA-STD program. A satisfactory match between the experimental and observed data was obtained, thus providing further evidence for the goodness of the TR-NOESY/STD-docking approach employed herein (see below).

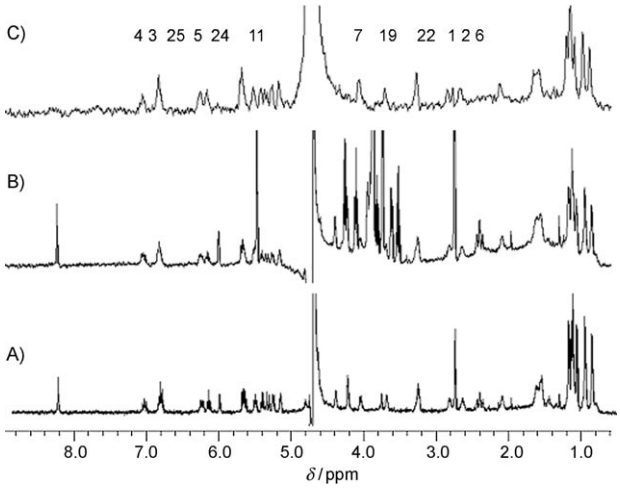


Figure 10. A) $^1$H NMR (500 MHz) spectrum of free dictyostatin ($D_2O$, 298 K), with a baccatin/tubulin molar ratio of 15:1. B) $^1$H NMR spectrum of dictyostatin in the presence of microtubules ($D_2O$, 298 K), with a molar ratio of 20:1. C) STD spectrum (saturation time: 2 s) of this last sample. Clear enhancements are observed for most of the dictyostatin signals, whereas those of the nucleotide employed for stabilizing the microtubules are not observed (huge nucleotide/tubulin molar ratio).

**The interactions of DDM and DCT with tubulin as revealed by the docking procedure**: As mentioned above, the experimentally derived NMR conformation of DDM was docked onto β-tubulin[43] (PDB code: 1JFF) as already described[35] and as explained in the Experimental Section, by using the AUTODOCK program.[42]

However, it has to be noted that two binding sites have been described for taxanes, the final luminal binding site, which has been experimentally proved for paclitaxel and epothilone, and an external transient binding site of unknown structure, that has been experimentally proved for cyclostreptin. Since it is not proved that dictyostatin and discodermolide reach the final internal luminal site, they might compete with paclitaxel by just binding to the free external site. Thus, the docking results have to be taken with caution. Indeed, the determined bound conformation is very similar to that described by Carlomagno and co-workers[31] with tubulin in a nonmicrotubule form, for which the luminal site might not be fully present or structured.

First, a global search for binding sites in the α/β-tubulin dimer was carried out, with a grid spacing of 0.6 Å. Because all of the binding modes obtained in this calculation were located at the region of β-tubulin that faces inside the microtubule, the second step involved a local search for the β-tubulin monomer, with a grid spacing of 0.375 Å.

The local docking for β-tubulin suggested that there is a preferred DDM-binding region within this monomer, since most of the 100 structures could be gathered in the lowest energy cluster. In fact, this binding site corresponds to the taxane-binding site[59] involving the α helices 6 and 7 and the β strands 8–10 with their corresponding loops (Figure 11). This model predicts no evident contacts with either helix 1 or 5.

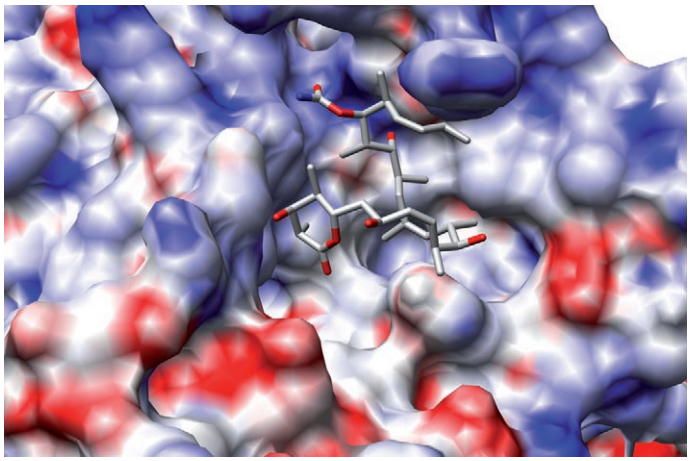

Figure 11. The interaction of DDM with β-tubulin, as deduced by AUTODOCK. The NMR-derived bound conformation of DDM was used with the refined coordinates of tubulin from PDB file 1JFF. The binding site perfectly correlates with the taxane-binding site. The charges at the protein surface were estimated by using Poisson–Boltzmann electrostatic calculations with the PDB2PQR program.[62,63]

There are a variety of nonpolar intermolecular contacts between DDM and tubulin. According to this binding mode, there are polar contacts of the ligand with His229 (helix 7), several residues at the M loop (Pro274, Thr276, Ser277, and Gln282), and Gly370. His229 is a key residue in the middle of helix 7. Stabilizing van der Waals interactions (within 5 Å of DDM) are also found, especially with Leu217, Leu275, Pro360, and Leu371 (the coordinates of the modeled DDM–tubulin complex are available from the authors upon request). It has been reported[31,60] that, in contrast to paclitaxel, DDM conserves full activity on cell lines presenting the F270V and A364T mutations. Indeed, no major contacts are found between DDM and these residues in our complex.

It is possible to speculate how this MSA exerts its function. Interestingly, in our model, DDM (and DCT, see below) directly contacts with the M loop. This M loop has been shown to be a key element of the lateral interactions

  

between microtubule protofilaments.[59,60] This evidence suggests the possibility that DDM stabilizes microtubules by stabilizing lateral contacts between protofilaments, as has been previously proposed for taxol.

The docking analysis was also performed for DCT by following the same methodology described for DDM. Indeed, an identical binding site was also deduced, which can fit the deduced NMR-bound conformer of DCT and that of DDM (Figure 12). DCT interacts with polar contacts again with

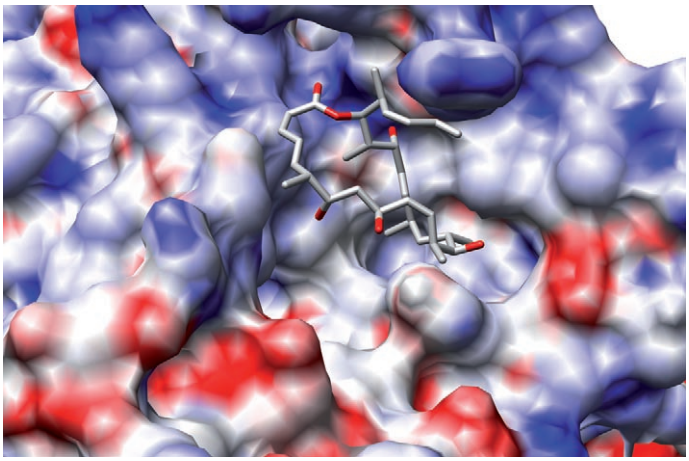

Figure 12. The interaction of DCT with β-tubulin, as deduced by AUTODOCK. The NMR-derived bound conformation of DCT was used with the refined coordinates of tubulin from PDB file 1JFF. The binding site perfectly correlates with the taxane-binding site. The charges at the protein surface were estimated by using Poisson–Boltzmann electrostatic calculations with the PDB2PQR program.[62,63]

His229, Pro274 (at the M loop), Thr276, Arg278, Gln282, and Gly370. For this macrocyclic molecule, which has a larger hydrophobic chain than DDM, a higher number of van der Waals interactions take place, namely with Leu217, Leu219, Leu230, Ala233 at helix 7, Leu275, and Leu371, with those residues providing the more important nonpolar contacts (within 5 Å of DCT). Thus, for both DDM and DCT, the two independently NMR-derived conformations for the assembled microtubule-bound state perfectly fit within the same binding site, as can be observed in Figure S12 in the Supporting Information. The intermolecular contacts observed for DCT with tubulin were indeed very similar to those described above for DDM, as can be observed from the superimposition of both molecules at the binding site.

Nevertheless, despite the fact that according to the combination of experimental and AUTODOCK data, both molecules target the taxane-binding site, the paclitaxel-binding pocket is not completely occupied by DDM or DCT. Superpositions of the three bound ligands are presented in Figure 13 and in the graphical abstract; these show that DDM and DCT roughly overlap the taxane skeleton but do not make the additional contacts provided by the docetaxel side chain, specifically with helix 1 and the other side of

Figure 13. Superimposition of the NMR-derived bound conformers of DDM and DCT, as deduced by AUTODOCK, with paclitaxel, as described in the coordinates of the PDB file 1JFF for the β-tubulin complex. In this case, the protein has been removed for the sake of clarity. There are still possibilities for the extension of DDM and DCT to provide additional contacts with the target receptor.

His229. It may be speculated that, if this model were correct, addition of a proper paclitaxel or docetaxel side chain to DCM or DCT might further stabilize their binding by about $-3$ kcal mol$^{-1}$ (from a comparison of the affinities of baccatin and paclitaxel, see reference [61]).

## Conclusion

A variety of NMR spectroscopic data, including TR-NOESY/STD, qualitative line-broadening analysis, and NMR competition experiments, assisted by molecular mechanics calculations, has been employed to deduce the microtubule-bound conformation of two MSAs, DDM, and DCT. The data indicate that tubulin in assembled microtubules recognizes DDM through a conformational selection process, in which the half-chair conformer (and not the skew-boat form that is predominant in solution) of the lactone moiety is bound by the receptor. There are very minor changes in the rest of the molecular skeleton between the major conformer in water solution and that bound to assembled microtubules. Indeed, despite the many torsional degrees of freedom of DDM, intramolecular interactions within the molecule and hydration strongly affect its conformational features, and it only shows conformational mobility around a fairly narrow part of the molecule. This evidence strongly contrasts with the observations in other solvents. Yet, this feature serves to modulate the presentation of polar and nonpolar surfaces to interact with the binding site of tubulin. With regard to DCT, its microtubule-bound conformation has also been derived by using the same combined protocol of NMR spectroscopy and molecular docking. The deduced bound geometry presents some key conformational differences, with respect to the major one existing in solution, around certain torsion angles and additionally displays mobility (even when bound) along the lateral C22–C26 diene chain. In any case, the bound conformer of DCT resembles that of DDM and provides very similar contacts with the receptor. Competition experiments have indicated that both molecules compete with the taxane-binding site, thereby providing further support to previously described biochemical data.

  

A model of the binding mode of both MSAs to tubulin, involving the taxane-binding site of tubulin, has been postulated. A hypothesis for both the major polar and nonpolar interactions between both MSA compounds (DDM and DCT) and the receptor has also been proposed.

The employed approach should be of general use within this field. Moreover, this experimental determination of the conformation of a microtubule-stabilizing agent when bound to microtubules in solution should be helpful for the design of analogues with improved activity.

## Acknowledgement

We thank the Ministery of Education and Science of Spain and Comunidad Autonoma de Madrid for funding (grant nos. CTQ2006-10874-C02-01 to J.J.-B., BIO2007-61336 to J.F.D., and BIPPED S-BIO-0214-2006 to J.M.A., J.F.D., and J.J.-B.). Dr. R. Campos provided generous access to the Bruker AVANCE 700 MHz spectrometer of CNIO (Madrid, Spain). We thank Prof. N. R. Krishna (University of Birmingham, AL, USA) for the use of the CORCEMA program for TR-NOESY and STD analysis and Dr. A. Olson (Scripps Research Institute, CA, USA) for providing AutoDock and auxiliary programs. I.P. thanks the Engineering and Physical Sciences Research Council and AstraZeneca (CASE studentship to N.M.G.) for funding.

[1] P. B. Schiff, J. Fant, S. B. Horwitz, *Nature* **1979**, *277*, 665–667.
[2] F. Gueritte-Voegelein, D. Guenard, F. Lavelle, M. T. Le Goff, L. Mangatal, P. Potier, *J. Med. Chem.* **1991**, *34*, 992–998.
[3] T. Mitchison, M. Kirschner, *Nature* **1984**, *312*, 237–242.
[4] M. A. Jordan, L. Wilson, *Nat. Rev. Cancer* **2004**, *4*, 253–265.
[5] B. Tan, D. Piwnica-Worms, L. Ratner, *Curr. Opin. Oncol.* **2000**, *12*, 450–458.
[6] J. A. Shabbits, R. Krishna, L. D. Mayer, *Expert Rev. Anticancer Ther.* **2001**, *1*, 585–594.
[7] L. He, G. A. Orr, S. B. Horwitz, *Drug Discovery Today* **2001**, *6*, 1153–1164.
[8] D. M. Bollag, P. A. McQueney, J. Zhu, O. Hensens, L. Koupal, J. Liesch, M. Goetz, E. Lazarides, C. M. Woods, *Cancer Res.* **1995**, *55*, 2325–2333.
[9] E. Hamel, D. L. Sackett, D. Vourloumis, K. C. Nicolaou, *Biochemistry* **1999**, *38*, 5490–5498.
[10] R. J. Kowalski, P. Giannakakou, S. P. Gunasekera, R. E. Longley, B. W. Day, E. Hamel, *Mol. Pharmacol.* **1997**, *52*, 613–622.
[11] Z. Wang, D. Yang, A. K. Mohanakrishnan, P. E. Fanwick, P. Nampoothiri, E. Hamel, M. Cushman, *J. Med. Chem.* **2000**, *43*, 2419–2429.
[12] M. C. Edler, R. M. Buey, R. Gussio, A. I. Marcus, C. D. Vanderwal, E. J. Sorensen, J. F. Díaz, P. Giannakakou, E. Hamel, *Biochemistry* **2005**, *44*, 11525–11538.
[13] I. Paterson, R. Britton, O. Delgado, A. Meyer, K. G. Poullennec, *Angew. Chem.* **2004**, *116*, 4729–4733; *Angew. Chem. Int. Ed.* **2004**, *43*, 4629–4633.
[14] D. E. Pryor, A. O'Brate, G. Bilcer, J. F. Díaz, Y. Wang, M. Kabaki, M. K. Jung, J. M. Andreu, A. K. Ghosh, P. Giannakakou, E. Hamel, *Biochemistry* **2002**, *41*, 9109–9115.
[15] T. N. Gaitanos, R. M. Buey, J. F. Díaz, P. T. Northcote, P. Teesdale-Spittle, J. M. Andreu, J. H. Miller, *Cancer Res.* **2004**, *64*, 5063–5067.
[16] R. M. Buey, I. Barasoain, E. Jackson, A. Meyer, P. Giannakakou, I. Paterson, S. Mooberry, J. M. Andreu, J. F. Díaz, *Chem. Biol.* **2005**, *12*, 1269–1279.
[17] E. Nogales, M. Whittaker, R. A. Milligan, K. H. Downing, *Cell* **1999**, *96*, 79–88.
[18] J. F. Díaz, I. Barasoain, J. M. Andreu, *J. Biol. Chem.* **2003**, *278*, 8407–8419.
[19] J. F. Díaz, I. Barasoain, A. A. Souto, F. Amat-Guerri, J. M. Andreu, *J. Biol. Chem.* **2005**, *280*, 3928–3937.
[20] R. M. Buey, E. Calvo, I. Barasoain, O. Pineda, M. C. Edler, R. Matesanz, G. Cerezo, C. D. Vanderwal, B. W. Day, E. J. Sorensen, J. A. Lopez, J. M. Andreu, E. Hamel, J. F. Díaz, *Nat. Chem. Biol.* **2007**, *3*, 117–125.
[21] B. Sato, H. Nakajima, Y. Hori, M. Hino, S. Hashimoto, H. Terano, *Jpn. J. Antibiot.* **2000**, *53*, 204–206.
[22] J. H. Nettles, H. Li, B. Cornett, J. M. Krahn, J. P. Snyder, K. H. Downing, *Science* **2004**, *305*, 866–869.
[23] E. ter Haar, R. J. Kowalski, E. Hamel, C. M. Lin, R. E. Longley, S. P. Gunasekera, H. S. Rosenkranz, B. W. Day, *Biochemistry* **1996**, *35*, 243–250.
[24] G. Pettit, Z. Cichacz, F. Gao, M. Boyd, J. Schmidt, *J. Chem. Soc. Chem. Commun.* **1994**, 1111–1112.
[25] I. Paterson, R. Britton, O. Delgado, A. E. Wright, *Chem. Commun.* **2004**, 632–633.
[26] I. Paterson, N. M. Gardner, *Chem. Commun.* **2007**, 49–51.
[27] L. A. Martello, M. J. LaMarche, L. He, T. J. Beauchamp, A. B. Smith, S. B. Horwitz, *Chem. Biol.* **2001**, *8*, 843–855.
[28] L. A. Martello, H. M. McDaid, D. L. Regl, C. P. Yang, D. Meng, T. R. Pettus, M. D. Kaufman, H. Arimoto, S. J. Danishefsky, A. B. Smith III, S. B. Horwitz, *Clin. Cancer Res.* **2000**, *6*, 1978–1987.
[29] S. Honore, K. Kamath, D. Braguer, S. B. Horwitz, L. Wilson, C. Briand, M. A. Jordan, *Cancer Res.* **2004**, *64*, 4957–4964.
[30] S. Honore, K. Kamath, D. Braguer, L. Wilson, C. Briand, M. A. Jordan, *Mol. Cancer Ther.* **2003**, *2*, 1303–1311.
[31] V. M. Sanchez-Pedregal, K. Kubicek, J. Meiler, I. Lyothier, I. Paterson, T. Carlomagno, *Angew. Chem.* **2006**, *118*, 7443–7447; *Angew. Chem. Int. Ed.* **2006**, *45*, 7388–7394.
[32] J. F. Díaz, M. Menéndez, J. M. Andreu, *Biochemistry* **1993**, *32*, 10067–10077.
[33] A. B. Smith III, M. J. LaMarche, M. Falcone-Hindley, *Org. Lett.* **2001**, *3*, 695–698.
[34] E. Monteagudo, D. O. Cicero, B. Cornett, D. C. Myles, J. P. Snyder, *J. Am. Chem. Soc.* **2001**, *123*, 6929–6930.
[35] J. Jiménez-Barbero, A. Canales, P. T. Northcote, R. M. Buey, J. M. Andreu, J. F. Díaz, *J. Am. Chem. Soc.* **2006**, *128*, 8757–8765.
[36] I. Paterson, G. J. Florence, K. Gerlach, J. Scott, N. Sereinig, *J. Am. Chem. Soc.* **2001**, *123*, 9535–9544.
[37] I. Paterson, O. Delgado, G. J. Florence, I. Lyothier, M. O'Brien, J. P. Scott, N. Sereinig, *J. Org. Chem.* **2005**, *70*, 150–160.
[38] A. A. Hyman, S. Salser, D. N. Drechsel, N. Unwin, T. J. Mitchison, *Mol. Biol. Cell* **1992**, *3*, 1155–1167.
[39] Macromodel, Version 9.1, Schrödinger, LLC, New York, NY, **2005**.
[40] N. L. Allinger, Y. H. Yuh, J. H. Lii, *J. Am. Chem. Soc.* **1989**, *111*, 8551–8566.
[41] W. C. Still, A. Tempczyk, R. C. Hawley, T. Hendrickson, *J. Am. Chem. Soc.* **1990**, *112*, 6127–6129.
[42] G. M. Morris, D. S. Goodsell, R. S. Halliday, R. Huey, W. E. Hart, R. K. Belew, A. J. Olson, *J. Comput. Chem.* **1998**, *19*, 1639–1662.
[43] J. Lowe, H. Li, K. H. Downing, E. Nogales, *J. Mol. Biol.* **2001**, *313*, 1045–1057.
[44] H. M. Berman, J. Westbrook, Z. Feng, G. Gilliland, T. N. Bhat, H. Weissig, I. N. Shindyalov, P. E. Bourne, *Nucleic Acids Res.* **2000**, *28*, 235–242.
[45] A. Bax, D. G. Davis, *J. Magn. Reson.* **1985**, *65*, 355–360.
[46] G. Bodenhausen, D. J. Ruben, *Chem. Phys. Lett.* **1980**, *69*, 185–189.
[47] T. L. Hwang, A. J. Shaka, *J. Am. Chem. Soc.* **1992**, *114*, 3157–3159.
[48] A. Kumar, R. R. Ernst, K. Wuthrich, *Biochem. Biophys. Res. Commun.* **1980**, *95*, 1–6.
[49] A. Poveda, J. L. Asensio, M. Martín-Pastor, J. Jiménez-Barbero, *J. Biomol. NMR* **1997**, *10*, 29–43.
[50] H. N. B. Moseley, E. V. Curto, N. R. Krishna, *J. Magn. Reson. Ser. B* **1995**, *108*, 243–261.
[51] V. Jayalakshmi, T. Biet, T. Peters, N. R. Krishna, *J. Am. Chem. Soc.* **2004**, *126*, 8610–8611.
[52] S. R. Arepalli, C. P. J. Glaudemans, G. D. Daves, P. Kovac, A. Bax, *J. Magn. Reson. Ser. B* **1995**, *106*, 195–198.

  

[53] J. L. Asensio, J. F. Espinosa, H. Dietrich, F. J. Cañada, R. R. Schmidt, M. Martín-Lomas, S. Andre, H. J. Gabius, J. Jiménez-Barbero, *J. Am. Chem. Soc.* **1999**, *121*, 8995–9000.
[54] B. Neuhaus, M. P. Williamson, *The Nuclear Overhauser Effect in Structural and Conformational Analysis*, VCH, New York, **1989**.
[55] J. Jiménez-Barbero, F. Amat-Guerri, J. P. Snyder, *Curr. Med. Chem. Anti-Cancer Agents* **2002**, *2*, 91–122.
[56] F. Ni, *Progr. NMR Spectrosc.* **1994**, *26*, 517–606.
[57] M. Mayer, B. Meyer, *J. Am. Chem. Soc.* **2001**, *123*, 6108–6117.
[58] B. Meyer, T. Peters, *Angew. Chem.* **2003**, *115*, 890–918; *Angew. Chem. Int. Ed.* **2003**, *42*, 864–890.
[59] J. P. Snyder, J. H. Nettles, B. Cornett, K. H. Downing, E. Nogales, *Proc. Natl. Acad. Sci. U.S.A.* **2001**, *98*, 5312–5316.
[60] H. Li, D. J. DeRosier, W. V. Nicholson, E. Nogales, K. H. Downing, *Structure* **2002**, *10*, 1317–1328.
[61] I. Barasoain, J. M. Andreu, *Biochemistry* **2001**, *40*, 11975–11984.
[62] N. A. Baker, D. Sept, S. Joseph, M. J. Holst, A. McCammon, *Proc. Natl. Acad. Sci. U.S.A.* **2001**, *98*, 10037–10041.
[63] T. J. Dolinsky, J. E. Nielsen, J. A. McCammon, N. A. Baker, *Nucleic Acids Res.* **2004**, *32*, 665–667.

Received: January 9, 2008
Published online: April 30, 2008

  